Noname manuscript No.
(will be inserted by the editor)

Abdominal artery segmentation method from CT volumes using fully convolutional neural network

Masahiro Oda · Holger R. Roth · Takayuki Kitasaka · Kazunari Misawa · Michitaka Fujiwara · Kensaku Mori

Received: 29 August 2018 / Accepted: 27 August 2019

Abstract *Purpose* The purpose of this paper is to present a fully automated abdominal artery segmentation method from a CT volume. Three-dimensional (3D) blood vessel structure information is important for diagnosis and treatment. Information about blood vessels (including arteries) can be used in patient-specific surgical planning and intra-operative navigation. Since blood vessels have large inter-patient variations in branching patterns and positions, a patient-specific blood vessel segmentation method is necessary. Even though deep-learning-based segmentation methods provide good segmentation accuracy among large organs, small organs such as blood vessels

M. Oda · H.R. Roth
Graduate School of Informatics, Nagoya University,
Furo-cho, Chikusa-ku, Nagoya, Aichi, Japan
Tel.: +81-(0)52-789-5688
Fax: +81-(0)52-789-3815
E-mail: moda@mori.m.is.nagoya-u.ac.jp

T. Kitasaka
School of Information Science, Aichi Institute of Technology,
1247 Yachigusa, Yagusa-cho, Toyota, Aichi, Japan

K. Misawa
Aichi Cancer Center,
1-1 Kanokoden, Chikusa-ku, Nagoya, Aichi, Japan

M. Fujiwara
Nagoya University Graduate School of Medicine,
65 Tsurumai-cho, Syouwa-ku, Nagoya, Aichi, Japan

K. Mori
Graduate School of Informatics, Nagoya University,
Research Center for Medical Bigdata, National Institute of Informatics,
2-1-2 Hitotsubashi, Chiyoda-ku, Tokyo, Japan

are not well segmented. We propose a deep-learning-based abdominal artery segmentation method from a CT volume. Because the artery is one of small organs that is difficult to segment, we introduced an original training sample generation method and a three-plane segmentation approach to improve segmentation accuracy.
Method Our proposed method segments abdominal arteries from an abdominal CT volume with a fully convolutional network (FCN). To segment small arteries, we employ a 2D patch-based segmentation method and an area imbalance reduced training patch generation (AIRTPG) method. AIRTPG adjusts patch number imbalances between patches with artery regions and patches without them. These methods improved the segmentation accuracies of small artery regions. Furthermore, we introduced a three-plane segmentation approach to obtain clear 3D segmentation results from 2D patch-based processes. In the three-plane approach, we performed three segmentation processes using patches generated on axial, coronal, and sagittal planes and combined the results to generate a 3D segmentation result.
Results The evaluation results of the proposed method using 20 cases of abdominal CT volumes show that the averaged F-measure, precision, and recall rates were 87.1%, 85.8%, and 88.4%, respectively. This result outperformed our previous automated FCN-based segmentation method. Our method offers competitive performance compared to the previous blood vessel segmentation methods from 3D volumes.
Conclusions We developed an abdominal artery segmentation method using FCN. The 2D patch-based and AIRTPG methods effectively segmented the artery regions. In addition, the three-plane approach generated good 3D segmentation results.

Keywords Abdominal artery · CT image · Segmentation · Fully convolutional network

1 Introduction

The abdominal arteries supply blood flow to many organs. The three-dimensional (3D) position and structure information of blood vessels (including arteries) is important for diagnosis and treatment. Since blood vessel information is used to identify organ positions [1,2] and to analyze cancer metastasis in diagnosis, such information is critical in surgical assistance. Surgeons control the blood flow in the operative field by clamping blood vessels, and blood vessel information guides them to identify the target blood vessels for clamping. If blood vessel information is poorly understood by surgeons, blood vessels might be damaged during surgery. Such trouble happens in laparoscopic surgeries due to distorted anatomy [3] and the limited viewing field of laparoscopes. Blood vessel information reduces complications. Various methods for assisting laparoscopic surgeries utilizing blood vessel information have been proposed [4–7]. Abdominal blood vessels have large inter-patient variations in branching

patterns, branch positions, and branch lengths. If patient-specific blood vessel information is obtained prior to surgery, surgeons can confirm the blood vessel positions and structures in pre-operative surgery simulations. This information is also used to perform intra-operative navigation [5,6] that indicates blood vessel positions during surgery. Therefore, the patient-specific 3D position and structure information of abdominal blood vessels, including arteries, is important.

Deep learning techniques, which have significantly impacted the medical image processing field, have also been applied to organ segmentation from medical images, where they have achieved high segmentation accuracy [16–18]. Deep learning techniques are expected to improve blood vessel segmentation performance. Most current deep-learning-based blood vessel segmentation methods have been applied to segmentation from 2D images. Many approaches have been proposed to segment retinal blood vessels from retinal images [19–25]. Among these, convolutional neural networks (CNNs) [19–22] and fully convolutional networks (FCNs) [23–25] have been utilized. The positional variation of the blood vessels in retinal images is limited compared to that of blood vessels in 3D volumes. Therefore, segmentation of the retinal blood vessels is relatively easy to perform.

Many blood vessel segmentation methods from medical images have been proposed [8,9], including 3D segmentation methods using model fitting [10, 11], the Hessian-based enhancement filter [12,13], and Sequential Monte Carlo tracking [14]. Recently, blood vessel segmentation methods from 3D volumes, such as computed tomography (CT) and magnetic resonance (MR) volumes, have been proposed [26–30]. Chen et al. [26] proposed an artery segmentation method from MR volumes of the brain. They employed a 3D patch (small image) based segmentation approach using an original FCN having a position input path. The position and shape of the arteries in the brain may have relationships to the positions in a MR volume. Therefore, they added a patch position input path to their FCN. The FCN has an encoder-decoder style similar to the 3D U-Net [31]. The sensitivity of their result was low, indicating that many false negatives were produced. From this result, patch position information is not useful for improving segmentation accuracy. Tetteh et al. [27] proposed a blood vessel segmentation method from MR volumes of the brain. They employed a 2D patch-based segmentation approach. The 2D patch is made by combining multiple images in a sequence of slices in a volume. They used an FCN without skip connection, which can be seen in the U-Net [34]. The skip connection is important to reflect spatial information to the segmentation results. Nardelli et al. [28] proposed a pulmonary artery and vein segmentation method from CT volumes. They used CNNs to segment the blood vessels and then apply the graph-cut to refine the results. The pulmonary blood vessels have clear contrast to the surrounding air region. The difficulty of their segmentation lies in the differentiation of blood vessels and small airways. Kitrungrotsakul et al. [29,30] proposed hepatic blood vessel segmentation methods from CT volumes. They also employed patch-based

segmentation approaches. Their segmentation target was the blood vessels in the liver region.

Deep-learning-based blood vessel segmentation from 3D volumetric images, including CT or MR volumes, is difficult due to the significant imbalance of volumes between blood vessels and other regions. Deep learning networks, which are trained to output a pixel-wise label value from a spatial intensity distribution on a CT volume, minimize the differences between the estimated and ground truth label values by minimizing a loss function. This is commonly performed in organ segmentation methods from CT volumes using FCNs [16, 17]. In these methods, large organs such as the liver and spleen are segmented with high accuracy. However, the blood vessels were not well segmented, which means that small blood vessels were not segmented and the segmented regions were fragmented into many regions. This result was caused by the significant volume imbalance between blood vessels and other regions. The blood vessels occupy a very small volume in CT volumes. Abdominal arteries occupy about 0.2% of the volume in the abdominal CT volumes in our dataset. Figure 1 shows examples of abdominal artery regions. Abdominal artery regions indicated by red are small in the CT volume. Commonly used loss functions such as the cross entropy loss fail to adequately reflect the existence of small regions [32,33]. Since deep learning networks tend to be trained to correctly segment regions with larger volumes, the segmentation accuracy of blood vessel regions is low.

To deal with the problem caused by the significant imbalance of volumes between blood vessels and other regions, we developed two strategies: a three-plane approach combining 2D patch-based segmentation processes and an area imbalance reduced training patch generation (AIRTPG) method. These two strategies provide accurate segmentation of blood vessels including small to large parts. Consequently, we solve the volume imbalance problem using these strategies. Other approaches tried to solve this problem by introducing loss functions having weights to reduce the effect of volume imbalance [33]. Generalized Dice loss is popular among them. However, finding their optimal weight values is difficult, and use of sub-optimal weight values reduces segmentation accuracy.

We propose a fully automated abdominal artery segmentation method from a CT volume using the two strategies described above. Our method uses an FCN, which is an image-to-organ likelihood regression network that estimates organ likelihood at each voxel in an input image. We tested FCNs, which are modified versions of U-Net [34], to perform segmentation. We utilize a small 2D patch based segmentation process to increase the occupancy of the artery regions in images. The use of small patches helps to improve segmentation accuracy. We also apply the AIRTPG method to create patches for FCN training. This method adjusts the imbalance of areas between artery and non-artery regions in patches and maintains high segmentation accuracy for small targets in the patch-based segmentation approach. In the segmentation process, the three-plane approach obtains good 3D segmentation results. This approach performs segmentation processes using patches generated on the ax-

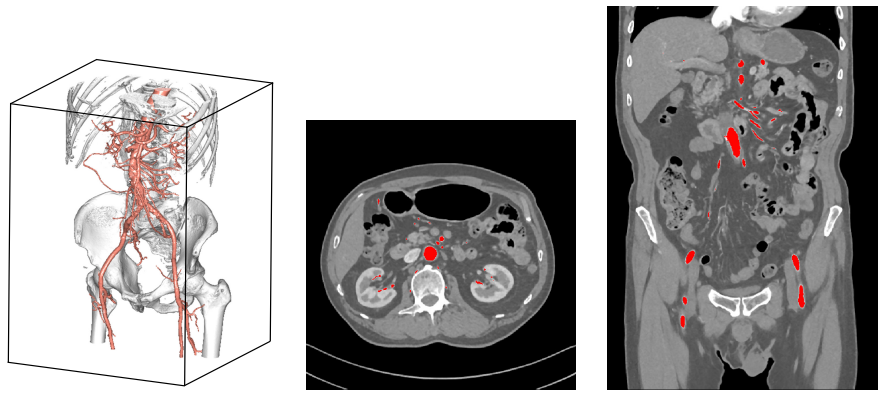

(a) (b) (c)

Fig. 1 Examples of abdominal artery regions in CT volume: (a) 3D volume rendered image. Artery regions are shown as red. Black frames indicate corners of CT volume. (b) and (c) axial and coronal slice images.

ial, coronal, and sagittal planes. Consequently, three segmentation results are combined to obtain a 3D segmentation result.

A preliminary report related to our proposed method was published at a conference [35]. The report [35] was included in the conference proceedings published as a supplemental issue of IJCARS. This method does not utilize any area imbalance reduction between the artery and non-artery regions in the patch generation; it only utilizes patches generated on the axial plane. The segmentation accuracy of the method [35] was low, and the segmented regions were fragmented into many regions. In the proposed method, these problems were solved by introducing the AIRTPG method and the three-plane approach in the segmentation process. AIRTPG reduces the class imbalance of training samples found in the preliminary report. This contributes to improving the segmentation accuracy of small targets such as an artery. We obtained higher segmentation accuracy and clearer 3D artery segmentation results with these methods.

2 Artery segmentation method

2.1 Overview

The proposed method segments the artery region from an arterial phase contrasted abdominal CT volume. We use a U-Net based FCN to perform the segmentation. The proposed method consists of training and segmentation parts (Fig. 2). In the training part, three FCNs are trained to perform segmentation using patches generated on the axial, coronal, and sagittal planes. After the training part, we performed artery-region segmentation from a CT volume. Patch-based segmentations were performed using the three FCNs. The

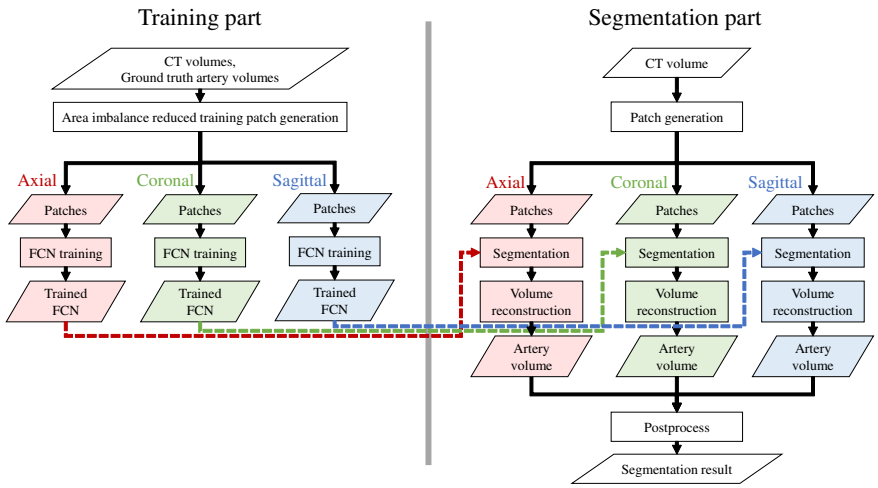

Fig. 2 Flowchart of artery segmentation method: Red, green, and blue process and data blocks use patches generated on axial, coronal, and sagittal planes, respectively.

patch-based segmentation results are reconstructed to make an artery-region segmentation result volume.

2.2 Training part

2.2.1 Area imbalance reduced training patch generation (AIRTPG)

Patches are generated as 2D clipped images on the axial, coronal, or sagittal planes from CT volumes and ground truth artery volumes. If the patches are clipped from these volumes in a uniform interval of positions, the number of patches containing artery regions becomes too small. The FCN cannot extract enough features to perform artery segmentation from such patches. To solve this problem, we generate about the same number of *artery* and *non-artery patches*. An *artery patch* contains an artery pixel at the center pixel of the patch. The center pixel of the *non-artery patch* is a non-artery pixel. These patches are generated at voxels in the volumes that meet the above condition. To generate about the same number of *artery* and *non-artery patches*, we densely and sparsely sample patches from artery and non-artery pixels, respectively.

We used a set of artery and non-artery patches for FCN training. Among them, patches generated from the CT volumes are called CT patches and those generated from ground truth artery volumes are called label patches. The intensity values in the patch are normalized to take values within 0 to 1. The intensity values of the label patches are 1 in the artery regions and 0 in the other regions.

2.2.2 Patch generation using AIRTPG

We use a set of training CT volumes and ground truth artery volumes. A median smoothing filter of a $3 \times 3 \times 3$-voxel size is applied to the CT volumes. We generated CT and label patches of $s \times s$ voxels from these volumes on the axial, coronal, and sagittal planes using the AIRTPG method. A set of patches generated on the axial plane is described as $P_a = \{I_a, L_a\}$, where I_a is a set of CT patches and L_a is a set of label patches. The sets of patches generated on the coronal and sagittal planes are also defined as P_c and P_s.

2.2.3 FCN training

We use FCNs to perform segmentation. We make three FCNs and train them to perform segmentation using patches generated on the axial, coronal, and sagittal planes using P_a, P_c, and P_s, respectively. The FCNs are trained to output a label patch from a CT patch given to the FCNs. The optimization algorithm of the FCNs is Adam [40]. We use binary cross entropy as the loss function that is minimized in the optimization. The minibatch size is set to 100. We experimentally selected the number of epochs in training. We performed experiments using 15 cases of CT volumes for training and five cases of CT volumes for evaluation, they were used in 3.1. We performed segmentations using the CT volumes for evaluation. We calculated the rate of matched voxels (between segmentation results and the ground truth) among all voxels. Among our experiments using different epoch numbers, training in 25 epochs gave good value of the rate of matched voxels. The FCNs are trained in 25 epochs. The FCN structures used here are explained below.

U-Net with batch normalization U-Net [34] is one of the FCNs used for segmentation. In the original paper [34], cell segmentation was performed from microscopic images. After U-Net's proposal, many U-Net-based segmentation methods were proposed [36–39]. U-Net-based networks performed segmentation from CT, MR, and laparoscopic images, demonstrating that U-Net is applicable to segmentation from various image modalities.

We use an FCN based on U-Net to perform artery segmentation in patches. The network structure is shown in Fig. 3 (a). The left part consists of convolution and max-pooling layers called the analysis path, which extracts features for segmentation from the input image. The right part consists of convolution and up-convolution layers called the synthesis path, which generates output images from the features. We added batch normalization after each convolution layer, which normalizes the mean and variance of features propagating the network. The use of batch normalization can reduce overfitting of the network to the training data.

Shallow U-Net with batch normalization Because the size of the patch is small, shallow FCN may extract enough features from the patches to perform segmentation. We made an FCN that has a U-Net-like structure but with a smaller

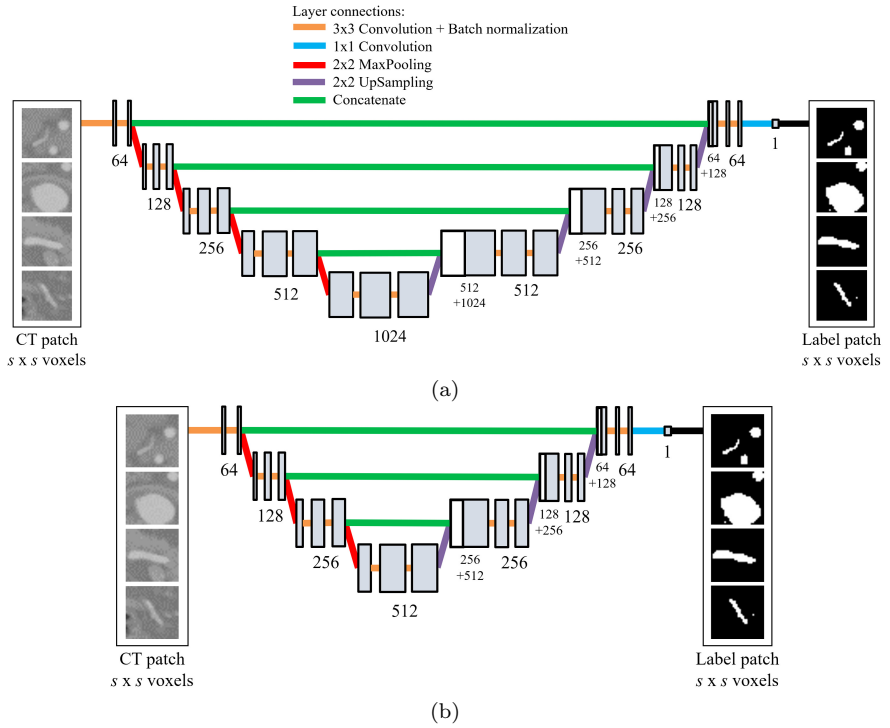

Fig. 3 FCN structures. (a) U-Net with batch normalization and (b) shallow U-Net with batch normalization. FCN network structure for patch-based artery segmentation: Boxes in network represent sets of feature maps. Numbers shown under boxes indicate amounts of feature maps or kernels.

number of layers than in its original structure. The network structure is shown in Fig. 3 (b).

U-Net with residual unit The residual unit is used to improve the performances of CNNs and FCNs. We used the Deep Residual U-Net [41], which has residual units in the U-Net structure.

2.3 Segmentation part

Three segmentation processes that use patches generated on the axial, coronal, and sagittal planes are carried out separately. As an example, we explain a segmentation process using patches that were generated on axial planes. Similar processes were also performed using patches generated on coronal and sagittal planes.

2.3.1 Patch generation

We perform a segmentation for a CT volume by applying a median $3 \times 3 \times 3$-voxel sized smoothing filter to it.

We generate CT patches by clipping 2D images on axial planes from the CT volume. The size of the CT patch is $s \times s$ pixels. The CT patches are clipped from an axial plane in the CT volume at $(x, y) = (s/2, s/2)$-pixel strides. x and y are mutually perpendicular coordinate axes aligned along the axial plane. We apply this clipping process to all of the axial planes in the CT volume. The intensity values in the CT patches are normalized to take values from 0 to 1.

2.3.2 Segmentation

We use FCN for the axial plane to perform patch-based segmentation. The CT patches are given to the FCN, which gives as output the estimated label patches.

2.3.3 Volume reconstruction

We reconstruct estimated label patches to a volume with the same size as the CT volume using the correspondence between a CT patch (used to estimate a label patch) and its clipped position in the CT volume. A pixel value in an estimated label patch is copied to the value of a voxel at a corresponding position in the reconstructed volume. Estimated label patches are overlapped up to four times in the reconstruction process (Fig. 4). We calculate the average pixel value in the overlapped patches to use as a voxel value in the reconstructed volume. By using the estimated label patches, we can obtain a reconstructed volume that contains a 3D artery segmentation result. We call this the artery volume obtained using patches on axial planes.

We also applied segmentation processes using patches generated on coronal and sagittal planes, thus allowing us to obtain three artery volumes generated with patches on the axial, coronal, and sagittal planes.

2.3.4 Postprocess

The three artery volumes are combined into a segmentation result volume by storing the maximum intensity value among them to the segmentation result volume at each voxel. We apply threshold value t to the segmentation result volume as well as dilation and erosion operations (structure element: sphere of radius r mm) to the regions in the volume to smoothen them. Among the remaining regions, we removed the connected components whose volume is smaller than v mm^3. The result of these processes is the final segmentation result.

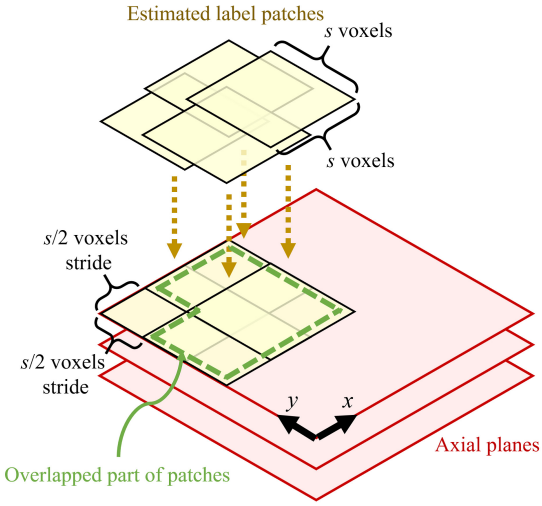

Fig. 4 Reconstruction of volume from 2D estimated label patches: 2D estimated label patches ($s \times s$ voxels) are aligned on axial planes with strides of $s/2$ voxels. Pixel value in estimated label patch is copied to value of voxel in volume at corresponding position. In overlapped parts of patches, average pixel values are copied to values of voxel in volume.

3 Experiments and Results

3.1 Experimental settings

The proposed method was evaluated using 20 cases of arterial phase-contrasted abdominal CT volumes whose acquisition parameters were as follows: 512×512 pixel image size, 753–1051 slices, 0.63–0.78 mm pixel spacing, and 1.0 mm slice spacing. The ground truth artery volumes were manually made. The parameters in the postprocess were set at $t = 0.75$, $r = 2$ mm, and $v = 200$ mm^3.

The FCNs were trained using 15 cases of the CT volumes. About 300,000 patches were generated from these CT volumes and used in the training process. Because we have a large number of patches, no data augmentation technique was used. We performed the artery segmentation process using the five remaining cases of CT volumes.

We used an NVIDIA TITAN V GPU equipped in a Windows 10 PC (CPU: Intel Xeon E5-2667 v4 3.2GHz, RAM: 64GB). We used the Keras to perform the training and inference of FCNs. Training and inference times are shown in Table 1.

We used the precision rate, the recall rate, and the F-measure (Dice coefficient) as the evaluation criteria of segmentation accuracy and defined them as

$$Precision = \frac{TP}{TP + FP}, \tag{1}$$

Table 1 Training and inference times of FCNs. Times are averages of processing times of patches generated on axial, coronal, and sagittal planes. U-Net BN: U-Net with batch normalization, S U-Net BN: shallow U-Net with batch normalization, and U-Net res: U-Net with residual unit [41]. s =32-voxel sized patches were used.

FCN structure	Training time (minutes)	Inference time (minutes)
U-Net BN	125.1	4.6
S U-net BN	83.5	3.0
U-Net Res	118.5	4.1

Table 2 Evaluation results of artery segmentation method. Results were compared among three patch sizes.

	F-measure (%)			Precision rate (%)			Recall rate (%)		
Patch size	Ave.	Min.	Max.	Ave.	Min.	Max.	Ave.	Min.	Max.
s =32	87.1	83.3	89.3	85.8	80.9	89.0	88.4	85.5	90.4
s =48	86.9	82.6	89.0	86.1	80.1	89.9	87.6	84.3	89.8
s =64	86.4	83.2	88.2	83.9	79.2	87.1	89.0	86.2	92.0

$$Recall = \frac{TP}{TP + FN}, \tag{2}$$

$$F - measure = 2\frac{Precision \cdot Recall}{Precision + Recall}, \tag{3}$$

where TP, FP, and FN are the numbers of the true positive, false positive, and false negative voxels in a segmentation result, respectively.

3.2 Evaluation using three patch sizes

We evaluated the segmentation accuracies of the proposed method using different sizes of patches: s =32, 48, and 64 voxels. The size of the smallest patch, s =32 voxels, is close in value to the diameter of the largest abdominal artery (aorta). The larger patches contain more tissue regions surrounding the artery than the smaller patches. These three sizes of patches were selected to confirm the relationships between segmentation accuracies and the textures of the artery and surrounding regions in patches. Examples of the patches are shown in Fig. 5.

The accuracies of the artery segmentation results for five cases of CT volumes are shown in Table 2 using the three patch sizes. We found small differences in accuracies among the three patch sizes. The highest averaged F-measure was obtained using the smallest patch size of $s = 32$ voxels. These accuracies were F-measure: 87.1%, precision rate: 85.8%, and recall rate: 88.4%.

The segmented regions are shown in Figs. 6 and 7. Most of the artery regions were segmented by the proposed method. The segmented artery regions were three-dimensionally connected components, representing not only a branch's shape but also the connections between branches.

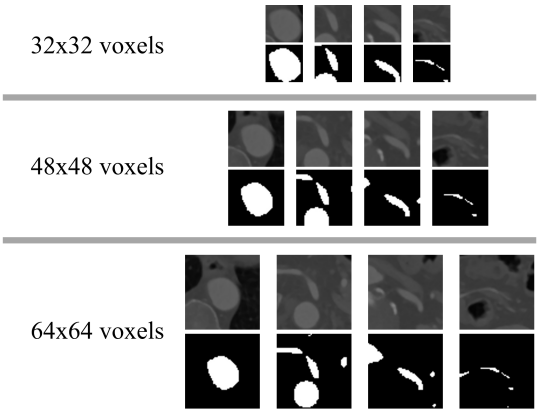

Fig. 5 Examples of three sizes of patches generated from axial planes. In each size, upper images are CT patches and lower binary images are label patches. Label patches are generated from ground truth artery regions as explained in 2.2.1. Larger patches contain more tissue regions surrounding an artery than smaller patches.

3.3 Evaluation using single- and three-patch planes

In the proposed method, we used patches that were generated on three planes: axial, coronal, and sagittal. We confirmed the effectiveness of the three-plane approach by comparing the results of two schemes: (1) the three-plane approach (proposed method) and (2) a single-plane approach. The single-plane approach, which employs a process flow that resembles the proposed method, uses only patches generated on the axial plane; it does not use any patch generated on the coronal or sagittal planes. We used patches of s =32 voxel size in this experiment.

The accuracies of the artery segmentation results using the two approaches are shown in Table 3. The averaged F-measure of the three-plane approach was higher than that of the single-plane approach. The overall segmentation performance of the three-plane approach was also higher. However, in the averaged precision rate, the single-plane approach showed higher performance; fewer FPs were generated in it. In the recall rate, the three-plane approach showed higher performance because it reduced the number of FNs.

The segmented regions are compared in Figs. 8 and 9. In these results, the single-plane approach failed to segment enough small arteries. The segmentation results of the three-plane approach contained many small artery regions.

3.4 Evaluation using three FCN structures

We confirmed the difference of segmentation accuracies using three FCN structures: (1) U-Net with batch normalization, (2) shallow U-Net with batch nor-

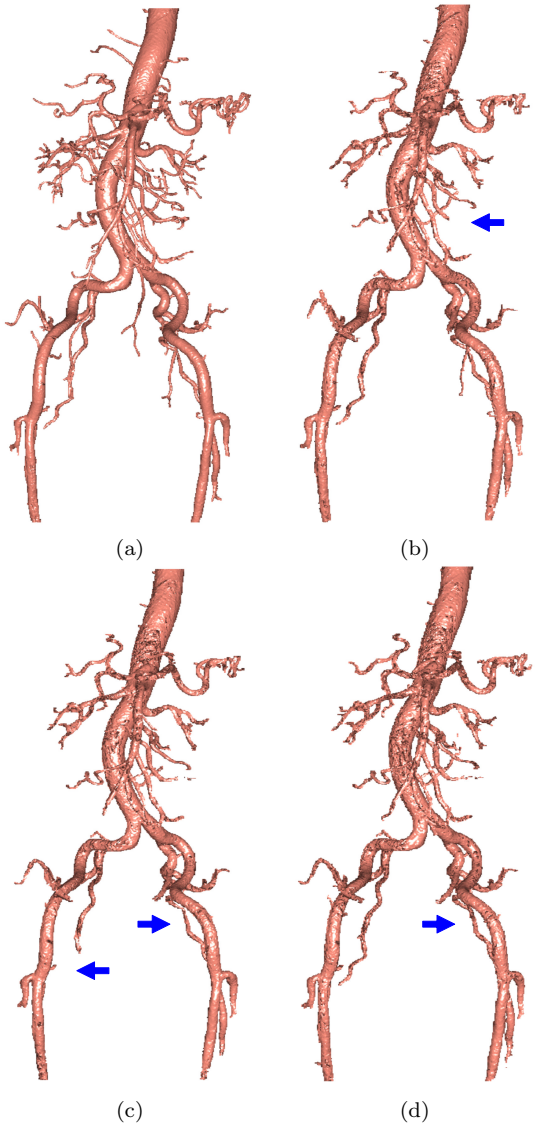

Fig. 6 Artery segmentation results of case 1: (a) ground truth. Segmentation results obtained using patch sizes: (b) $s = 32$, (c) $s = 48$, and (d) $s = 64$ voxels. The differences among three segmentation results are indicated by arrows. Some small arteries were not segmented.

malization, and (3) U-Net with residual unit [41]. We used patches of s =32 voxel size and the three-plane approach in this experiment.

The accuracies of the artery segmentation results using the three FCN structures are shown in Table 4. The difference of the accuracies between three

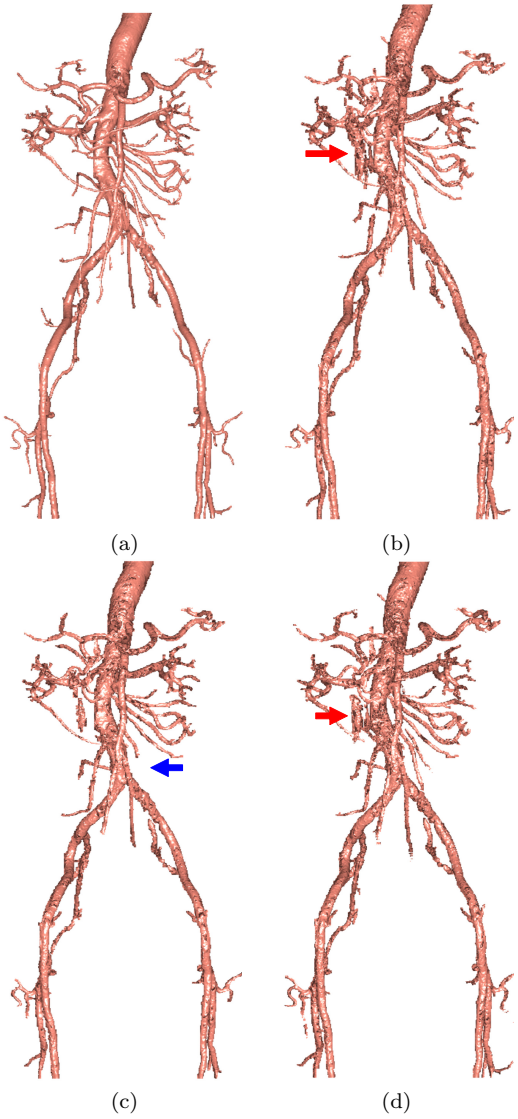

Fig. 7 Artery segmentation results of case 2: (a) ground truth. Segmentation results obtained using patch sizes: (b) $s = 32$, (c) $s = 48$, and (d) $s = 64$ voxels. The differences among three segmentation results are indicated by arrows. Red and blue arrows indicate false positives and unsegmented regions. The false positives are part of the vein regions.

FCN structures were very small. The U-Net with residual unit gave slightly higher accuracies among the FCNs.

Table 3 Evaluation results of three-plane approach (proposed method using patches generated on axial, coronal, and sagittal planes) and single-plane approach (patches generated on axial plane): s =32-voxel sized patches were used.

Approach	F-measure (%)			Precision rate (%)			Recall rate (%)		
	Ave.	Min.	Max.	Ave.	Min.	Max.	Ave.	Min.	Max.
Three-plane	87.1	83.3	89.3	85.8	80.9	89.0	88.4	85.5	90.4
Single-plane	83.2	78.8	86.3	92.7	89.1	94.6	75.5	67.7	79.7

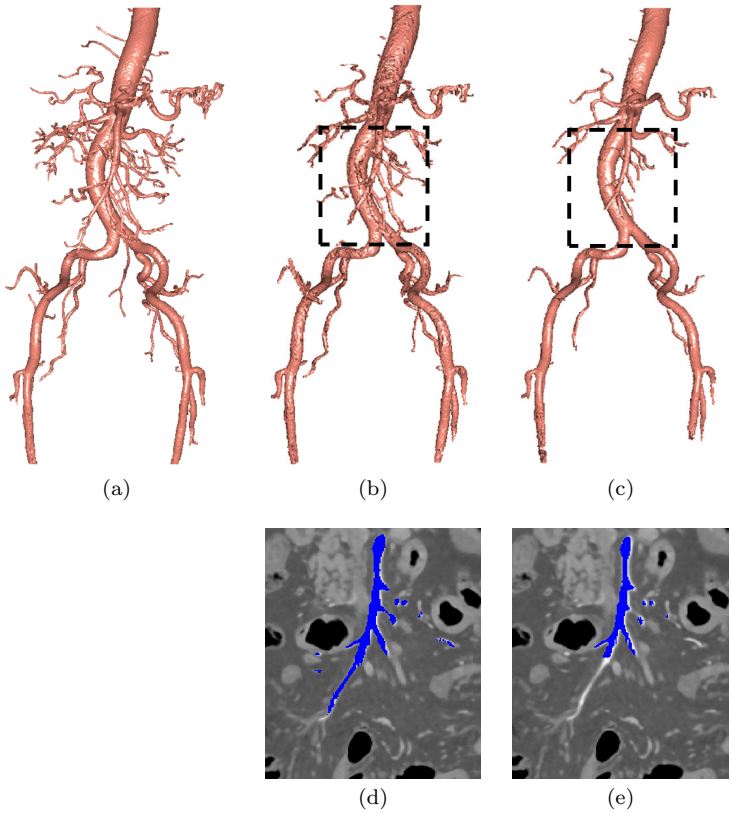

Fig. 8 Artery segmentation results of case 1: (a) ground truth. Segmentation results obtained using (b, d) three-plane approach and (c, e) single-plane approach. (d) and (e) are coronal slices showing segmentation results corresponding to boxed regions in (b) and (c).

4 Discussion

The proposed method segmented most of the artery regions from CT volumes. Because it employs a fully automated process, it can be used for diagnosis and surgical assistance. The segmentation accuracy of the previous semi-automated artery segmentation method [13] was 91.3% precision and 80.0% recall. The proposed method has greater competitive accuracy (precision rate: 85.9%, re-

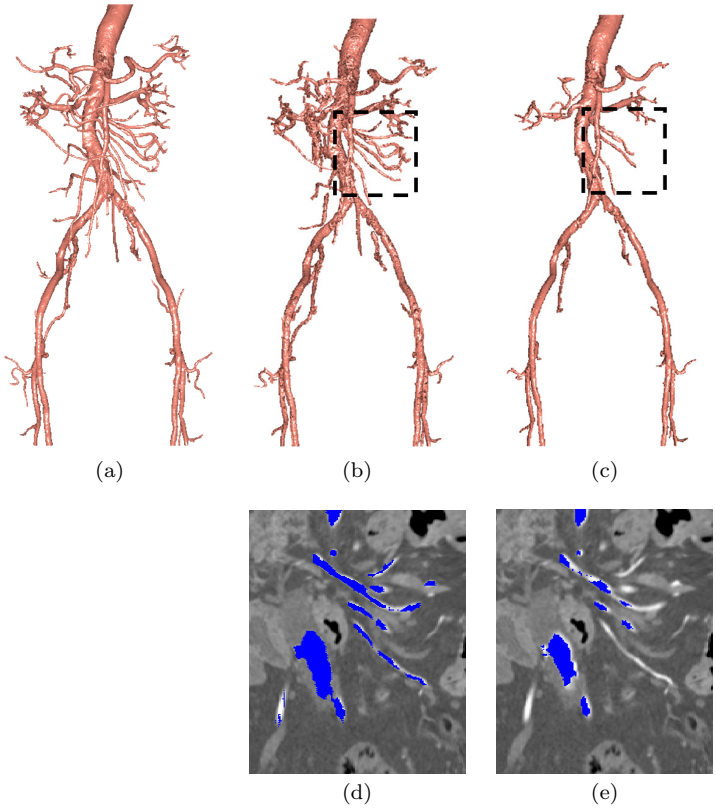

Fig. 9 Artery segmentation results of case 2: (a) ground truth. Segmentation results obtained using (b, d) three-plane approach and (c, e) single-plane approach. (d) and (e) are coronal slices showing segmentation results corresponding to boxed regions in (b) and (c).

Table 4 Evaluation results of three FCN structures. U-Net BN: U-Net with batch normalization, S U-Net BN: shallow U-Net with batch normalization, and U-Net res: U-Net with residual unit [41]. s =32-voxel sized patches and three-plane approach were used.

FCN structure	F-measure (%)			Precision rate (%)			Recall rate (%)		
	Ave.	Min.	Max.	Ave.	Min.	Max.	Ave.	Min.	Max.
U-Net BN	87.1	83.3	89.3	85.8	80.9	89.0	88.4	85.5	90.4
S U-Net BN	87.0	83.2	89.1	85.8	81.3	88.7	88.2	85.1	90.3
U-Net Res	87.2	83.0	89.5	85.9	80.5	88.8	88.5	85.4	90.9

call rate: 88.5%) compared to the previous method while also achieving complete automation. Because the proposed method employed a machine learning method, further improvement of segmentation accuracy would be expected if it were trained using more training data. The previous artery segmentation method using an FCN [35] obtained an 81.4% recall rate. Our proposed method has a higher recall rate than this previous method. Consequently, the

AIRTPG method and the three-plane approach improved segmentation accuracy. Among the previous blood vessel segmentation methods from 3D volumes [26–30], image modality and the segmentation target of the hepatic blood vessel segmentation methods proposed by Kitrungrotsakul et al. [29,30] are close to the proposed method. Their hepatic blood vessel segmentation accuracies were 83.0% [29] and 87.9% [30] in Dice coefficient (definition of the Dice coefficient is the same as the F-measure in voxel-wise comparison of regions). Our segmentation target contains arteries related to most of the abdominal organs. Their positions and branching patterns vary widely compared to blood vessels in a single organ. However, our proposed method still segmented arteries with competitive accuracy against the other methods. This means our proposed method has high segmentation performance.

We compared the segmentation results obtained using three patch sizes. The segmentation accuracies show little difference among the three patch sizes. Using the smallest patch ($s = 32$ voxels) resulted in the highest averaged F-measure. These results indicate that the area of the surrounding structures of the segmentation target in a patch is unrelated to segmentation accuracy. From the viewpoint of computational resource usage, the smallest patch is a reasonable choice because the required amounts of training time and memory consumption are small.

We used patches generated on three planes: axial, coronal, and sagittal. This three-plane approach resulted in a great reduction of FNs in the experimental results. The single-plane approach failed to segment enough small arteries (Figs. 8 (c,e) and 9 (c,e)). Segmenting small artery regions only from patches on the axial planes is difficult because many other tissues have similar texture patterns to small arteries. In such a case, artery specific texture patterns can be found in patches on the coronal or sagittal planes. Utilization of patches generated on the three planes improves the chances of finding artery-specific texture patterns. This resulted in a high averaged F-measure and recall rate. The precision rate decreased when we used the three-plane approach. This means more FPs were found in the result. The FPs include part of the vein region as shown in Figs. 7 (b) and (d). The trade-off between FN and FP voxel numbers are commonly discussed in segmentation. Among them, the reduction of FN has great importance because the chance of overlooking a target region must be reduced in medical applications. The three-plane approach reduced more FNs compared to the single-plane approach. We believe the three-plane approach generates better segmentation results for medical applications. Nevertheless, we need to reduce FPs by training FCNs using more patches of the vein regions as non-artery samples.

We compared the segmentation accuracies using three FCN structures. The accuracies in the all evaluation criteria, including the F-measure, the precision rate, and the recall rate, were almost same among the FCN structures. The shallow U-Net with batch normalization has the lowest F-measure. This means deeper networks are suitable for the segmentation. The U-Net with residual unit [41] has slightly higher accuracies among the FCN structures. This means the residual unit is effective for the segmentation.

From Table 1, the proposed method took 83.5 to 125.1 minutes to train the FCNs. The inference times were 3.0 to 4.6 minutes. Because we employed the small 2D patch-based segmentation process, the training and inference times were short. Furthermore, uses of the GPU memory of both the training and inference fit in the GPU memory sizes of common GPUs (8GB). This means the proposed method works with sufficiently short processing time even in normal computers. The proposed method can be deployed on computer systems in hospitals with small investment in equipment. The proposed method is suitable for practical use.

5 Conclusions

This paper proposed a fully automated abdominal artery segmentation method from CT volumes. The volumes of the artery regions are very small in the abdominal CT volumes. To segment artery regions, we employed a 2D patch-image-based segmentation method using FCNs. In our method, we processed 2D patches generated on axial, coronal, and sagittal planes to segment 3D artery regions. In our training patch generation, the AIRTPG method decreased the effect of a significant number imbalance between the artery and non-artery patches in the segmentation result. The FCNs were trained using the generated patches. In our segmentation process, these trained FCNs performed patch-based segmentation. The patches were reconstructed to a 3D volume to obtain a 3D segmentation result. In our experiments using 20 cases of CT volumes, the segmentation accuracies of the artery regions were 87.1% in F-measure, 85.8% in precision rate, and 88.4% in recall rate, all of which are competitive performances for a semi-automated segmentation method. Future work will use of 3D information in the patch-based segmentation process and introduce global blood vessel structure features in the segmentation process. Future work also involves developing applications for the segmentation of other blood vessels, including portal veins and other veins.

6 Ethical approval

For this type of study formal consent is not required.

7 Conflict of interest

The authors declare that they have no conflict of interest.

Acknowledgements Parts of this research were supported by MEXT, JSPS KAKENHI Grant Numbers 26108006, 17H00867, JSPS Bilateral International Collaboration Grants, and JST ACT-I (JPMJPR16U9).

References

1. Maklad AS, Matsuhiro M, Suzuki H, Kawata Y, Niki N, Shimada M, Iinuma G, Automatic blood vessel based-liver segmentation using the portal phase abdominal CT, Proceedings of SPIE Medical Imaging, 1057527, (2018)
2. Okada T, Linguraru MG, Hori M, Summers RM, Tomiyama N, Sato Y, Abdominal multi-organ CT segmentation using organ correlation graph and prediction-based shape and location priors, Medical Image Computing and Computer-Assisted Intervention (MICCAI), 8151, 275–282 (2013)
3. Nezhat C, Childers J, Nezhat F, Nezhat CH, Seidman DS, Major retroperitoneal vascular injury during laparoscopic surgery, Human Reproduction, 12(3), 480–483 (1997)
4. Amir-Khalili A, Peyrat JM, Abinahed J, Al-Alao O, Al-Ansari A, Hamarneh G, Abugharbieh R, Auto localization and segmentation of occluded vessels in robot-assisted partial nephrectomy, Medical Image Computing and Computer-Assisted Intervention (MICCAI), 8673, 407–414 (2014)
5. Hayashi Y, Misawa K, Oda M, Hawkes DJ, Mori K, Clinical application of a surgical navigation system based on virtual laparoscopy in laparoscopic gastrectomy for gastric cancer, International Journal of Computer Assisted Radiology and Surgery, 11(5), 827–836 (2016)
6. Ieiri S, Uemura M, Konishi K, Souzaki R, Nagao Y, Tsutsumi N, Akahoshi T, Ohuchida K, Ohdaira T, Tomikawa M, Tanoue K, Hashizumie M, Taguchi T, Augmented reality navigation system for laparoscopic splenectomy in children based on preoperative CT image using optical tracking device, Pediatric Surgery International, 28(4), 341–346 (2012)
7. Lee SW, Shinohara H, Matsuki M, Okuda J, Nomura E, Mabuchi H, Nishiguchi K, Takaori K, Narabayashi I, Tanigawa N, Preoperative simulation of vascular anatomy by three-dimensional computed tomography imaging in laparoscopic gastric cancer surgery, Journal of the American College of Surgeons, 197(6), 927–936 (2003)
8. Lesage D, Angelini ED, Bloch I, Funka-Lea G, A review of 3D vessel lumen segmentation techniques: models, features and extraction schemes, Medical Image Analysis, 13, 819–845 (2009)
9. Moccia S, Momi ED, Hadji SE, Mattos LS, Blood vessel segmentation algorithms – Review of methods, datasets and evaluation metrics, Computer Methods and Programs in Biomedicine, 158, 71–91 (2018)
10. Wörz S, Rohr K, Segmentation and quantification of human vessels using a 3-D cylindrical intensity model, IEEE Transactions on Image Processing, 16(8), 1994–2004 (2007)
11. Goyal A, Jack L, Lamata P, Wijngaard J, Horssen P, Spaan J, Siebes M, Grau V, Smith NP, Model-based vasculature extraction from optical fluorescence cryomicrotome images, IEEE Transactions on Medical Imaging, 32(1), 56–72 (2013)
12. Frangi AF, Niessen WJ, Vincken KL, Viergever MA, Multiscale vessel enhancement filtering, Medical Image Computing and Computer-Assisted Intervention (MICCAI), 1496, 130–137 (1998)
13. Oda M, Yamamoto T, Yoshino Y, Mori K, Segmentation method of abdominal arteries from CT volumes utilizing intensity transition along arteries, International Journal of Computer Assisted Radiology and Surgery, 11(1), S46–S47 (2016)
14. Cherry KM, Peplinski B, Kim L, Wang S, Lu L, Zhang W, Liu J, Wei Z, Summers RM, Sequential Monte Carlo tracking of the marginal artery by multiple cue fusion and random forest regression, Medical Image Analysis, 19(1), 164–175 (2015)
15. Sato Y, Westin C-F, Bhalerao A, Nakajima S, Shiraga N, Tamura S, Kikins R, Tissue classification based on 3D local intensity structures for volume rendering, IEEE Transactions on Visualization and Computer Graphics, 6(2), 160–180 (2000)
16. Roth HR, Oda M, Shimizu N, Oda H, Hayashi Y, Kitasaka T, Fujiwara M, Misawa K, Mori K, Towards dense volumetric pancreas segmentation in CT using 3D fully convolutional network, Proceedings of SPIE Medical Imaging 10574, 105740B-1–105740B-6 (2018)
17. Roth HR, Oda H, Zhou X, Shimizu N, Yang Y, Hayashi Y, Oda M, Fujiwara M, Misawa K, Mori K, An application of cascaded 3D fully convolutional networks for medical image segmentation, Computerized Medical Imaging and Graphics, 66, 90–99 (2018)

18. Zhou X, Takayama R, Wang S, Hara T, Fujita H, Deep learning of the sectional appearances of 3D CT images for anatomical structure segmentation based on an FCN voting method, Medical Physics, 44(10), 5221–5233 (2017)
19. Fu H, Xu Y, Lin S, Wong DWK, Liu J, DeepVessel: Retinal vessel segmentation via deep learning and conditional random field, Medical Image Computing and Computer-Assisted Intervention (MICCAI), 9901, 132–139 (2016)
20. Fu A, Xu Z, Gao M, Buty M, Mollura DJ, Deep vessel tracking: A generalized probabilistic approach via deep learning, IEEE 13th International Symposium on Biomedical Imaging (ISBI) (2016)
21. Liskowski P, Krawiec K, Segmenting retinal blood vessels with deep neural networks, IEEE Transactions on Medical Imaging, 35(11), 2369–2380 (2016)
22. Prentašic P, Heisler M, Mammo Z, Lee S, Merkur A, Navajas E, Beg MF, Šarunic M, Loncaric S, Segmentation of the foveal microvasculature using deep learning networks. Medical Image Computing and Computer-Assisted Intervention (MICCAI), 9901, 132–139 (2016)
23. Dasgupta A, Singh S, A fully convolutional neural network based structured prediction approach towards the retinal vessel segmentation. IEEE 14th International Symposium on Biomedical Imaging (ISBI) (2017)
24. Zhang Y, Chung ACS, Deep supervision with additional labels for retinal vessel segmentation task, Medical Image Computing and Computer-Assisted Intervention (MICCAI), 11071, 83–91, (2018)
25. Wu Y, Xia Y, Song Y, Zhang Y, Cai W, Multiscale network followed network model for retinal vessel segmentation, Medical Image Computing and Computer-Assisted Intervention (MICCAI), 11071, 119–126, (2018)
26. Chen L, Xie Y, Sun J, Balu N, Mossa-Basha M, Pimentel K, Hatsukami TS, Hwang J-N, Yuan C, Y-net: 3D intracranial artery segmentation using a convolutional autoencoder, arXiv:1712.07194 (2017)
27. Tetteh G, Efremov V, Forkert ND, Schneider M, Kirschke J, Weber B, Zimmer C, Piraud M, Menze BH, DeepVesselNet: Vessel segmentation, centerline prediction, and bifurcation detection in 3-D angiographic volumes, arXiv:1803.09340v2 (2018)
28. Nardelli P, Jimenez-Carretero D, Bermejo-Pelaez D, Washko GR, Rahaghi FN, Ledesma-Carbayo MJ, Estépar RSJ, Pulmonary artery-vein classification in CT images using deep learning, IEEE Transactions on Medical Imaging, 37(11), 2428–2440 (2018)
29. Kitrungrotsakul T, Han X-H, Iwamoto Y, Foruzan AH, Lin L, Chen W-Y, Robust hepatic vessel segmentation using multi deep convolution network, Proceedings of SPIE Medical Imaging, 1013711, (2017)
30. Kitrungrotsakul T, Han X-H, Wei X, Chen W-Y, Multi-pathways CNN for robust vascular segmentation, Proceedings of SPIE Medical Imaging, 105781S, (2018)
31. Çiçek Ö, Abdulkadir A, Lienkamp SS, Brox T, Ronneberger O, 3D U-net: learning dense volumetric segmentation from sparse annotation, Medical Image Computing and Computer-Assisted Intervention (MICCAI), 9901, 424–432, (2016)
32. Milletari F, Navab N, Ahmadi SA, V-net: Fully convolutional neural networks for volumetric medical image segmentation, Fourth International Conference on 3D Vision (3DV), 565–571, (2016)
33. Sudre CH, Li W, Vercauteren T, Ourselin S, Cardoso MJ, Generalised Dice overlap as a deep learning loss function for highly unbalanced segmentations, International Workshop on Deep Learning in Medical Image Analysis (DLMIA), 10553, 240–248, (2017)
34. Ronneberger O, Fischer P, Brox T, U-Net: convolutional networks for biomedical image segmentation, Medical Image Computing and Computer-Assisted Intervention (MICCAI), 9351, 234–241, (2015)
35. Oda M, Kitasaka T, Misawa K, Fujiwara M, Mori K, Abdominal artery segmentation from CT volumes using fully convolutional network for small artery segmentation, International Journal of Computer Assisted Radiology and Surgery, 13(1), S20–21 (2018)
36. Jin D, Xu Z, Harrison AP, George K, Mollura DJ, 3D convolutional neural networks with graph refinement for airway segmentation using incomplete data labels, Machine Learning in Medical Imaging (MLMI) 2017, 10541, 141–149 (2017)

37. Jang Y, Hong Y, Ha S, Kim S, Chang HJ, Automatic segmentation of LV and RV in cardiac MRI, Statistical Atlases and Computational Models of the Heart, ACDC and MMWHS Challenges, STACOM 2017, 10663,161–169 (2018)
38. Patravali J, Jain S, Chilamkurthy S, 2D-3D fully convolutional neural networks for cardiac MR segmentation, Statistical Atlases and Computational Models of the Heart, ACDC and MMWHS Challenges, STACOM 2017, 10663, 130–139 (2018)
39. Kurmann T, Simultaneous recognition and pose estimation of instruments in minimally invasive surgery, Medical Image Computing and Computer-Assisted Intervention (MICCAI), 10434, 505–513 (2017)
40. Diederik PK, Jimmy B, Adam: A method for stochastic optimization, arXiv:1412.6980 (2014)
41. Zhang Z, Liu Q, Wang Y, Road Extraction by Deep Residual U-Net, IEEE Geoscience and Remote Sensing Letters (2018)